Photoluminescence Excitation Spectroscopy of Diffused Layers on Crystalline Silicon Wafers

Hieu T. Nguyen, Sieu Pheng Phang, Jennifer Wong-Leung, and Daniel Macdonald

***Abstract*—Photoluminescence (PL) excitation spectroscopy is applied to observe the evolution of the luminescence spectra from dopant-diffused crystalline silicon wafers with varying excitation wavelength. Utilizing the micrometer-scale spatial resolution achievable with confocal optics in a micro-photoluminescence spectroscopy system, along with the well-resolved luminescence peaks at cryogenic temperatures from various defects and structures in a single-silicon substrate, we are able to examine the doping densities and junction depths of various boron-diffused wafers, as well as the distribution of defects induced underneath the wafer surface by the post-diffusion thermal treatment. Our conclusions are validated by photoluminescence scans and transmission electron microscopy applied to vertical cross sections, which confirm the presence of dislocations below the diffused regions.**

***Index Terms*—Crystalline silicon, diffusion process, excitation spectroscopy, photoluminescence (PL), photovoltaic cells.**

I. Introduction

PHOTOLUMINESCENCE spectroscopy (PLS) is a powerful technique to assess fundamental properties of crystalline silicon (c-Si), such as the temperature [1] and doping [2], [3] dependences of the band gap, the band-to-band absorption [4]–[6], radiative recombination [5], [7], [8], and donor–acceptor pair luminescence [9], [10]. Besides that, PLS-based methods have also been employed for precise and nondestructive characterization in silicon photovoltaics (PV), for example, to extract minority carrier diffusion lengths in c-Si wafers [11], [12] and bricks [13], to quantify the light-trapping capability of various plasmonic structures [14], or to examine the impacts of surface reflectance [15], [16] and different carrier profiles [16] on photoluminescence (PL) spectra. Recently, utilizing a micro-PLS (μPLS) system with micrometer-scale spatial resolution courtesy of confocal optics, spectroscopic properties of various microscopic defects and structures in c-Si wafers and solar cells have been studied, such as dislocations [17]–[19], iron precipitates [20], laser-doped regions [21]–[24], and locally diffused regions [25].

On the other hand, photoluminescence excitation (PLE) spectroscopy, in which the luminescence intensity at certain wavelengths is monitored with varying excitation wavelengths, has also been employed to study many fundamental properties of c-Si, such as the optical band gap in degenerate silicon [2], [26], oxygen-related deep defects in irradiated silicon [27], and isoelectronic bound excitons in beryllium-doped silicon [28]. Recently, Juhl *et al.* [29] applied a PLE-type method to capture the total PL emission from c-Si wafers in imaging mode, under two different excitation wavelengths, from which they were able to extract high-resolution images of the absolute absorptance of solar cell precursors.

In this work, we combine the two PL techniques mentioned above (PLS and PLE) and capture the entire band-to-band luminescence spectrum, while varying the excitation wavelength, with the measurements performed at cryogenic temperatures and with micrometer-scale spatial resolution. This spectrally resolved PLE technique is founded on the fact that the radiative recombination mechanism is generally different for each layer or defect type in a c-Si wafer, leading to distinct peaks in PL spectra at cryogenic temperatures. Furthermore, these components of the aggregate luminescence spectrum from a wafer composed of multiple layers are expected to have different dependences on the excitation wavelength, since the fraction of the excitation light absorbed in each layer varies with excitation wavelength. Therefore, by varying the excitation wavelengths, we can probe the layers and defects at different depths below the wafer surface, providing useful information about the spatial distribution of dopants and defects. First, we demonstrate this method on boron-diffused c-Si samples with various doping densities and junction depths. After that, we apply the method to detect and characterize specific defects induced underneath the wafer surface by the post-diffusion thermal treatment, highlighting some potential applications of the technique for silicon PV. The results are confirmed by μPLS measurements and transmission electron microscopy (TEM) performed on vertical cross sections of relevant samples.

II. Experimental Details

The samples studied in Section III are float-zone phosphorus-doped c-Si wafers with a resistivity of 100 Ω·cm. They were first chemically etched in a solution consisting of HF and HNO_3 to remove saw damage. After that, they were heavily doped with boron from a BBr_3 gas source between 900 and 1000 °C in a quartz tube furnace with various drive-in times in a pure oxygen environment to achieve different doping profiles in the diffused layers. More details about this diffusion process can be found in [30].

The samples studied in Sections IV and V are $\langle 1\ 0\ 0 \rangle$-oriented float-zone boron-doped c-Si wafers with a resistivity of

Manuscript received November 15, 2015; revised January 12, 2016; accepted February 11, 2016. This work was supported by the Australian Research Council and the Australian Renewable Energy Agency through Research Grant RND009.

H. T. Nguyen, S. P. Phang, and D. Macdonald are with the Research School of Engineering, The Australian National University, Canberra, A.C.T. 2601, Australia (e-mail: hieu.nguyen@anu.edu.au; pheng.phang@anu.edu.au; daniel.macdonald@anu.edu.au).

J. Wong-Leung is with the Department of Electronic Materials Engineering, The Australian National University, Canberra, A.C.T. 2601, Australia (e-mail: jenny.wongleung@anu.edu.au).

Color versions of one or more of the figures in this paper are available online at http://ieeexplore.ieee.org.

Digital Object Identifier 10.1109/JPHOTOV.2016.2532460

TABLE I
PROCESSING STEPS FOR THE SAMPLES INVESTIGATED IN SECTIONS IV AND V

	Sample names					
Processes (in sequence)	N1	N2	N3	O1	O2	O3
1. Boron-diffused at 1050 °C, 60 min	Yes	Yes	Yes	Yes	Yes	Yes
2. BSG layer was removed by diluted HF	Yes	Yes	No	Yes	Yes	No
3. BRL layer was removed by boiling HNO_3	Yes	No	No	Yes	No	No
4. Annealed at 1090 °C for 5 h	Yes, in N_2	Yes, in N_2	Yes, in N_2	Yes, in O_2	Yes, in O_2	Yes, in O_2
5. Both BSG and BRL layers were removed	Yes	Yes	Yes	Yes	Yes	Yes

"N" indicates the samples annealed in nitrogen and "O" indicates samples annealed in oxygen.

about 0.3 Ω·cm, corresponding to a background doping of 6×10^{16} cm^{-3}. They were first chemically etched in HF/HNO_3 to remove saw damage and then went through the thermal diffusion process in a BBr_3 gas source at 1050 °C for 60 min. The resultant borosilicate glass (BSG) and boron-rich layer (BRL) on the surface were either kept or removed by diluted HF (for removing the BSG layer) and boiling HNO_3 (for removing the BRL layer). After that, these samples were annealed in either pure nitrogen or oxygen gases at 1090 °C for 5 h. Any residual BSG and BRL layers were finally removed prior to performing the PL measurements. Table I summarizes the process steps for these samples. These process steps are, in general, impractical for solar cell applications. They are aimed to generate different types of defects separated at different depths below the wafer surface, which best illustrate the capabilities of the technique presented here.

The experimental setup of our μ-PLS system is described in detail elsewhere [31]. A supercontinuum excitation light source (NKT SuperK Extreme EXR-20) with a tunable wavelength range between 490 nm and 2 μm was employed. In this work, excitation wavelengths between 510 and 810 nm were used with a bandwidth of 10 nm for the chosen wavelengths, and the on-sample power was kept constant at 6 mW for all excitation wavelengths. The wavelength selection was achieved using a SuperK VARIA attachment allowing the tuning of both the center wavelength and the bandwidth of the filtered light. The diameter of the illuminated spot on the samples varied between $\sim$1 μm (for 510-nm excitation wavelength) and $\sim$2 μm (for 810-nm excitation wavelength). The spectral response of the entire system was determined with a calibrated halogen–tungsten light source. The measurement temperature was kept at 79 K using a liquid-nitrogen-cooled cryostat. The cross-sectional specimens for μPLS measurements were prepared by a conventional mechanical polishing technique, whereas the cross-sectional specimens for TEM were prepared by focused ion beam. TEM analysis was carried out in a Phillips CM300 instrument operated at 300 keV. The doping profiles of the diffused layers were measured using the electrochemical capacitance–voltage (ECV) technique.

III. SPECTRALLY RESOLVED PHOTOLUMINESCENCE EXCITATION ON DIFFUSED SILICON WAFERS

Fig. 1(a) shows doping profiles of two different boron-diffused samples measured by ECV. The doping profile of sample 1 is shallower but higher in concentration, compared with sample 2. Fig. 1(b) plots the absorption depth versus excitation wavelength in c-Si at 79 K. The data were calculated from [32] and the effects of heavy doping were neglected. Fig. 1(c) and (d) shows the evolution of normalized PL spectra of samples 1 and 2, respectively, with increasing excitation wavelengths from 510 to 810 nm at 79 K. Two distinct peaks can be observed in each spectrum. The peak located at $\sim$1130 nm is the band-to-band emission from the underlying c-Si substrate (denoted as c-Si peak) and was used for normalizing the spectra for different excitation wavelengths. The second peak at $\sim$1165 nm (sample 1) and $\sim$1157 nm (sample 2) is the band-to-band emission attributed to the heavily doped layer near the surface (denoted as HDBB peak) [24], [25]. Compared with the c-Si peak, this HDBB peak is shifted to longer wavelengths due to band-gap narrowing (BGN) effects in heavily doped silicon [2], [3]. At the shortest excitation wavelength (510 nm), a large fraction of the laser light is absorbed in the diffused layer near the surface. Therefore, the HDBB peak is intense compared with the c-Si peak. However, when the excitation wavelength increases, i.e., the absorption depth increases, the laser light is absorbed more in the silicon substrate but less in the diffused layer. Therefore, the relative intensity of the HDBB peak is suppressed, compared with the c-Si peak.

Fig. 2(a) compares the normalized spectra between the two samples at two excitation wavelengths: 510 and 810 nm. The first notable feature is the difference in the energy and width of the HDBB peak between the two samples. The HDBB peak of sample 1 is lower in energy (i.e., longer wavelength) and broader compared with that of sample 2, indicating that the diffused layer of sample 1 is more heavily doped than that of sample 2. The difference is explained by the illustration in Fig. 2(b). There are two distinct points for the heavily doped silicon: 1) the luminescence gap E_{g2} is smaller than that of the low-doped silicon E_{g1} due to BGN effects [2], [3]; and 2) the Fermi energy level E_F is shifted into the valence band E_V (for p-type doping), and thus, all energy states between E_F and E_V are occupied by free holes [26], [33]. Meanwhile, the free holes in low-doped silicon are very close to the valence band edge due to rapid carrier thermalization. Thus, the radiative recombination between the two band edges has a wider energy distribution in heavily doped silicon compared with lowly doped silicon [26], [33], [34]. Therefore, the higher the doping density in the diffused layer, the lower the energy and the broader the width of the HDBB peak. Note that the nonhomogeneous doping profile throughout the thickness of the diffused layer also contributes to the broadening of the HDBB peak, compared with the c-Si peak, which is emitted from the homogeneously doped substrate.

The second notable feature is the difference in the HDBB peak intensity between the two samples. The normalized HDBB peak of sample 1 is reduced more quickly than that of sample 2 when the laser light penetrates deeper into the substrate. This feature demonstrates that the junction depth of sample 2 is deeper than that of sample 1. Therefore, by employing this spectrally resolved PLE technique, one can qualitatively assess both the doping level and the junction depth of the heavily doped layers in c-Si wafers and solar cells. The technique is, in principle, only

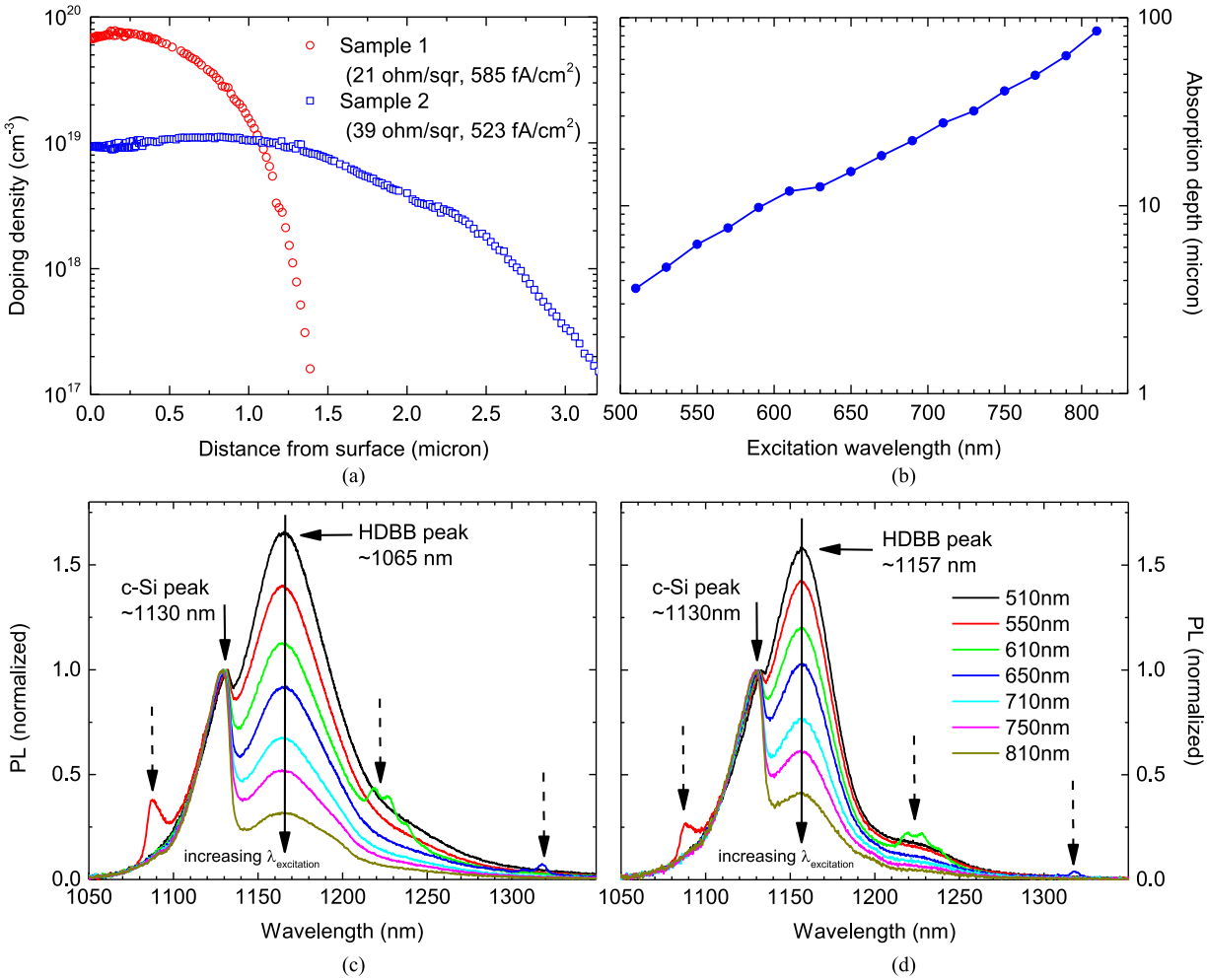

Fig. 1. (a) Doping profiles of the two boron-diffused samples. The numbers in brackets are the measured sheet resistance (using the four-point probe technique) and emitter saturation current density (see [30] for the measurement technique), respectively. (a) Absorption depth versus excitation wavelength in c-Si at 79 K. The data were calculated from [32], and the effects of heavy doping were neglected. PL spectra of (c) sample 1 and (d) sample 2, captured at 79 K with varying excitation wavelengths. All spectra were normalized to the c-Si peak. The spurious peaks marked by broken-line arrows are harmonic artifacts due to the not-entirely-suppressed sidebands of the supercontinuum laser.

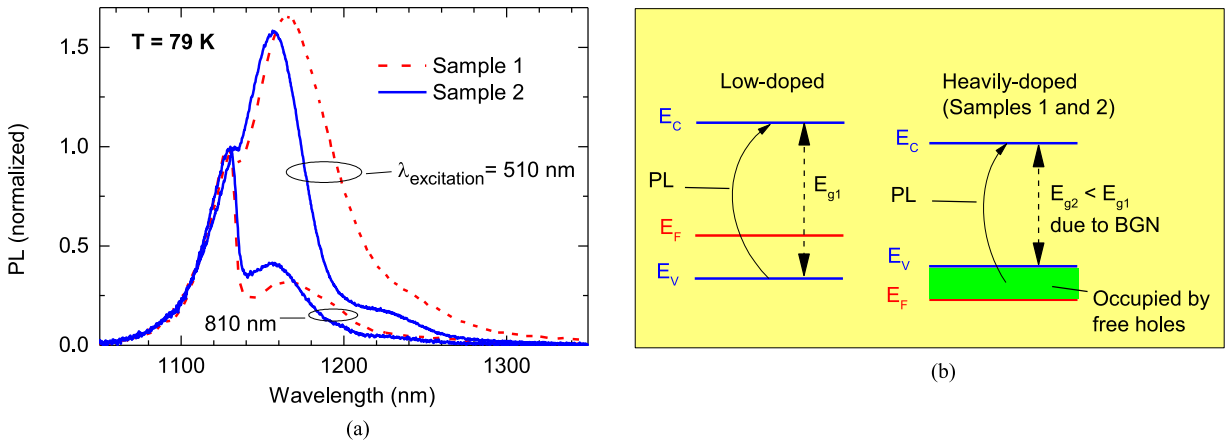

Fig. 2. (a) Comparison of normalized PL spectra between sample 1 and sample 2, excited with the 510- and 810-nm wavelengths at 79 K. All spectra were normalized to the c-Si peak. (b) Radiative recombination scheme in low-doped and heavily doped p-type c-Si wafers.

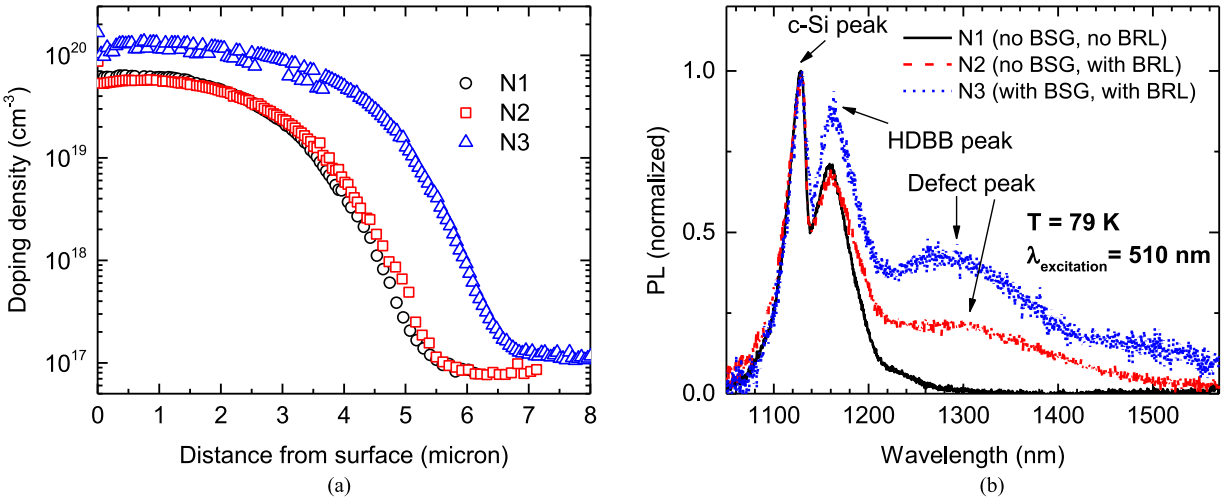

Fig. 3. (a) Doping profiles of three samples N1, N2, and N3. (b) Comparison of normalized PL spectra among the three samples, excited with the 510-nm wavelength at 79 K.

sensitive to active dopants since only active dopants contribute to the BGN effects, causing the HDBB peak. However, the absorption depth of the excitation light is expected to be smaller than the values presented in Fig. 1(b) due to the smaller effective band gap in heavily doped silicon. In addition, this parameter varies throughout the thickness of the diffused layer. Hence, we do not place an emphasis on calculating the exact junction depth from this technique at the current stage. Note that there is also a weak shoulder around 1230 nm, which is mostly visible in sample 2. This is the phonon replica of the HDBB peak.

IV. Spectrally Resolved Photoluminescence Excitation on Defects Induced by Post-Diffusion Thermal Treatment

In this section, we examine the impact of the post-diffusion thermal treatment on the formation of defects underneath the wafer surface, applying the spectrally resolved PLE technique. Fig. 3(a) plots the doping profiles of the three samples N1, N2, and N3 (see Table I for a description of these samples). As can be seen from this figure, sample N3 (retaining both BSG and BRL layers before annealing) is more heavily doped than the other two, since the BSG layer acts as a further source of boron doping, which diffuses into the silicon wafer during annealing at high temperatures [35]. Fig. 3(b) shows the normalized spectra from the three samples, excited with the 510-nm wavelength at 79 K. Besides the c-Si (from the silicon substrate) and HDBB (from the heavily doped region) peaks, samples N2 and N3 also show a strong deep-level luminescence peak at ~1300 nm. However, sample N1 (for which both the BRL and BSG layers were removed before being annealed) does not show any defect luminescence, despite having a similar doping profile with sample N2. The BSG layer was removed by diluted HF, in which silicon is not dissolved. The BRL layer was removed by oxidizing the wafers in boiling HNO_3 with 20-min intervals and was considered to be removed completely if the wafer surface was hydrophobic after HF dip. The boiling HNO_3 was demonstrated to oxidize less than 5 nm of silicon in 10 min [36], and thus, the 20-min interval oxidation causes no significant changes to the boron diffusion profiles across all samples. This suggests that the heavily doped layer itself, annealed at high temperatures, does not cause the observed deep-level luminescence.

Furthermore, we did not observe any defect luminescence from the three samples annealed in an oxygen environment O1, O2, and O3. Since the oxidation process converts the BRL layer into a BSG layer [35], the absence of defect luminescence from these samples suggests that annealing the BSG layer by itself does not cause deep-level defects inside the silicon wafers. These findings are consistent with the results reported by Cousins and Cotter [37] and Kessler *et al.* [38]. Cousins and Cotter found that their boron-diffused wafers were heavily dislocated when driving them in with an inert gas directly after the diffusion process (thus, the BRL layer was still present) but found minimal dislocations in the wafers driven in with an oxygen environment [37]. Kessler *et al.* reported that a thick BRL layer caused a bulk lifetime degradation of silicon wafers during the annealing and cooling process, and this degradation could be avoided by a drive-in step in oxygen gas to reverse the BRL formation [38]. Therefore, we propose that annealing the BRL layer causes a mechanical stress between this layer and the silicon wafer, creating dislocations that can glide into the silicon wafer and cause the deep-level luminescence. The type and origin of the deep-level luminescence, as well as the presence of dislocations, will be clarified in Section V.

Next, we demonstrate the application of the spectrally resolved PLE method on the defects induced by the post-diffusion thermal treatment mentioned above, giving us useful information about the depth distribution of different types of defects below the wafer surface. Fig. 4(a) and (b) shows the normalized spectra of samples N2 and N3 with varying excitation wavelengths at 79 K. As in Fig. 1(b) and (c), the longer the excitation wavelengths, the less pronounced the HDBB peak, compared with the c-Si peak. However, we can also observe a suppression of the defect peak with increasing excitation wavelengths,

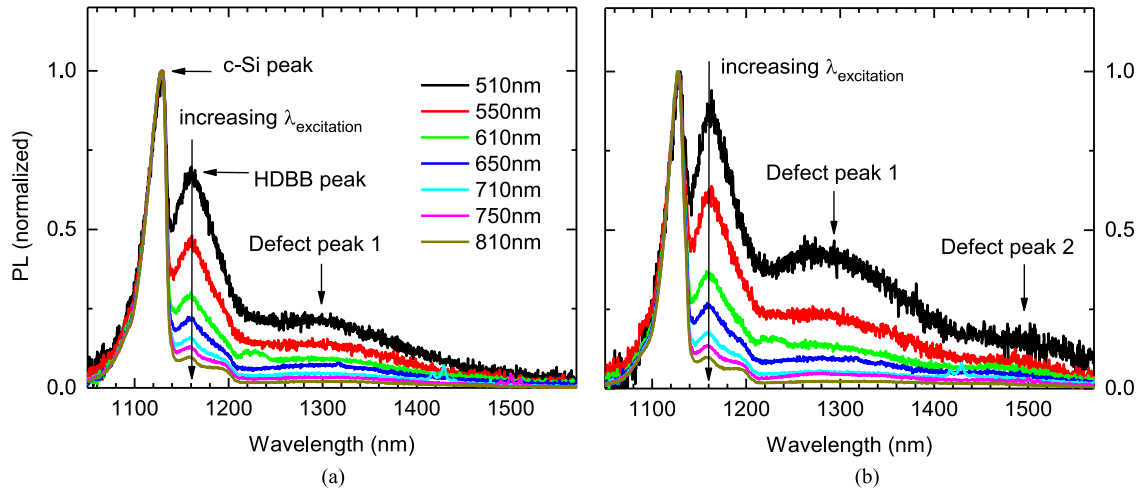

Fig. 4. PL spectra of (a) sample N2 and (b) sample N3, captured at 79 K with varying excitation wavelengths. All spectra were normalized to the c-Si peak.

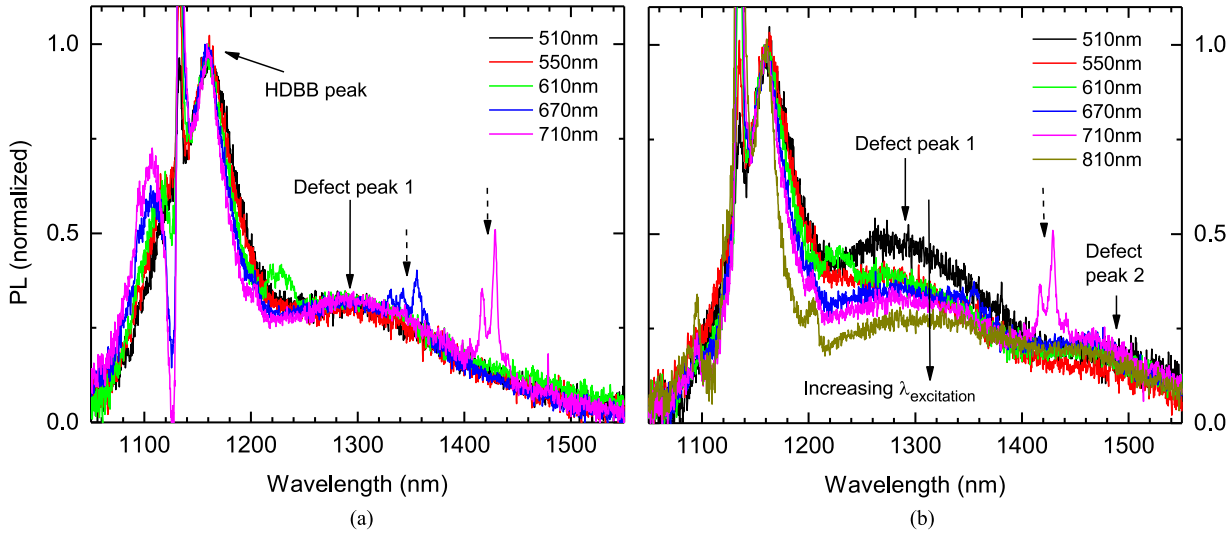

Fig. 5. PL spectra of (a) sample N2 and (b) sample N3, captured at 79 K with varying excitation wavelengths. The c-Si component was subtracted from all spectra, and the resultant spectra were normalized to the HDBB peak. The spurious peaks marked by broken-line arrows are harmonic artifacts due to the not-entirely-suppressed sidebands of the supercontinuum laser. The spectrum at 810-nm excitation wavelength was not shown in (a) since the HDBB peak was not well resolved after subtracting the c-Si component.

compared with the c-Si peak. Therefore, we conclude that the observed defect luminescence originates from the region near the wafer surface. Moreover, a detailed inspection of the defect luminescence reveals a difference between the two samples. Sample N2 has only one defect peak located at ∼1300 nm, whereas sample N3 seems to have another weak defect peak at ∼1480 nm. Therefore, we denoted the two peaks at ∼1300 and ∼1480 nm as "defect peak 1" and "defect peak 2," respectively, in Fig. 4(a) and (b).

Furthermore, Fig. 5(a) and (b) plots the spectra, normalized to the HDBB peak, of samples N2 and N3. The c-Si peak has been subtracted from all spectra in order to avoid the impact of this peak on the spectral components from the near surface region. In Fig. 5(a), the shape of the defect luminescence is very consistent, and there is only one peak for all excitation wavelengths. However, in Fig. 5(b), there are two different defect peaks at ∼1300 and ∼1480 nm, and their relative intensity is different from each other with increasing excitation wavelengths. Compared with defect peak 2, defect peak 1 is less pronounced when the laser light penetrates more deeply into the c-Si substrate. Therefore, these results suggest that although both defects are distributed near the surface region, defect peak 2 is distributed more deeply into the substrate than defect peak 1. Note that all spectra presented so far were measured from above the wafer surface, i.e., this method is nondestructive.

V. Verification of Defect Luminescence Using Cross-Sectional μPhotoluminescence Spectroscopy and Transmission Electron Microscopy

Now, we verify the findings regarding the spatial distribution of defect peaks 1 and 2 mentioned above, using the PL spectra captured from a vertical cross-sectional slice of the investigated boron-diffused c-Si wafers. The cross section was

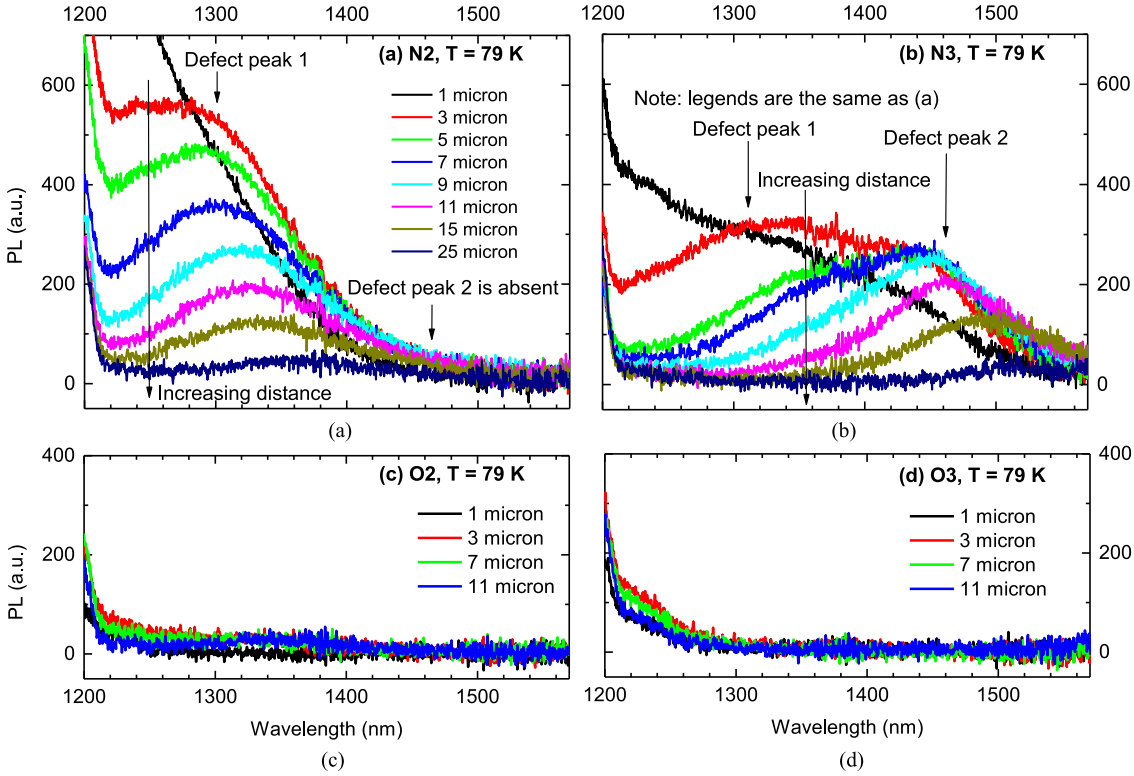

Fig. 6. PL spectra on the cross sections of samples (a) N2, (b) N3, (c) O2, and (d) O3, captured at 79 K with 810-nm excitation wavelength. The lengths indicate the distance from the original wafer surface on the cross section.

excited with the 810-nm wavelength to allow the laser light to penetrate deeply into the samples (from the cross-sectional view), thus reducing the nonradiative recombination caused by the damaged layer resulting from the mechanical polishing on the cross-sectional surface. Fig. 6(a) and (b) shows the relative PL spectra from samples N2 and N3, captured at different distances from the edge of the cross section (which is the original sample surface). As can be readily seen from Fig. 6(a), defect peak 2 is absent from all spectra, whereas the intensity of defect peak 1 reduces with increasing distances from the edge. However, in Fig. 6(b), we can observe unambiguously both defect peaks. The intensity of defect peak 1 reduces quickly, whereas that of defect peak 2 still remains strong up to a certain distance from the edge. Meanwhile, no defect luminescence is observed in the spectra from the samples annealed in an oxygen environment, as depicted in Fig. 6(c) and (d). The results from these four figures are consistent with our conclusions above.

In addition, comparing the two defect peaks with the so-called D lines emitted from dislocations, their spatial distributions are consistent with those of the doublets D3/D4 and D1/D2, respectively [18], [19], [31], [38]. The doublet D1/D2 was demonstrated to be emitted from the secondary defects and impurities trapped around dislocation sites, and thus, their spatial distribution is usually extended over a broader region around the dislocation sites [18], [19], [31], [38]. Meanwhile, the doublet D3/D4 was found to reflect the intrinsic properties of dislocations themselves, since the luminescence was confined to very near the dislocation sites [18], [19], [31], [39]. Therefore, we propose that defect peak 1 represents the doublet D3/D4, whereas defect peak 2 is expected to be the doublet D1/D2. Decomposing defect peaks 1 and 2 into their individual D lines is difficult, since these two peaks are emitted from the regions in which the doping profile is nonuniform, thus broadening the two peaks due to varying amount of BGN in heavily doped silicon. However, once the distance from the edge of the cross section is far enough [e.g., the 15-μm curve in Fig. 6(b)], the contribution from the uniform- and low-doped region dominates the spectrum and the position of defect peak 2 is similar to the reported D1 line [31], [39].

Finally, a TEM two-beam [–1 –1 1] bright-field image of the (0 1 1) cross section of the boron-diffused silicon wafer N3 is shown in Fig. 7(a) and (b) for low and high magnifications, respectively. The micrograph in Fig. 7(a) reveals a dislocation band located about 3 μm below the wafer surface. Between this dislocation band and the surface is a dislocation-free zone. This distribution of dislocations is similar to the results reported by Ning [40] and was explained by the movement of dislocations formed at the wafer surface during the annealing and cooling process. Therefore, the observed deep-level luminescence is likely to be related to the dislocations.

Since defect peak 2 was not present on samples N1 (annealed in nitrogen gas) and N2 (annealed in nitrogen gas with the BRL layer present), this defect peak is not likely to be due to either nitrogen diffused into the wafers or nitrogen–oxygen complexes [41]. Another possibility is that this defect peak could originate from oxygen precipitates, since its energy level is similar to

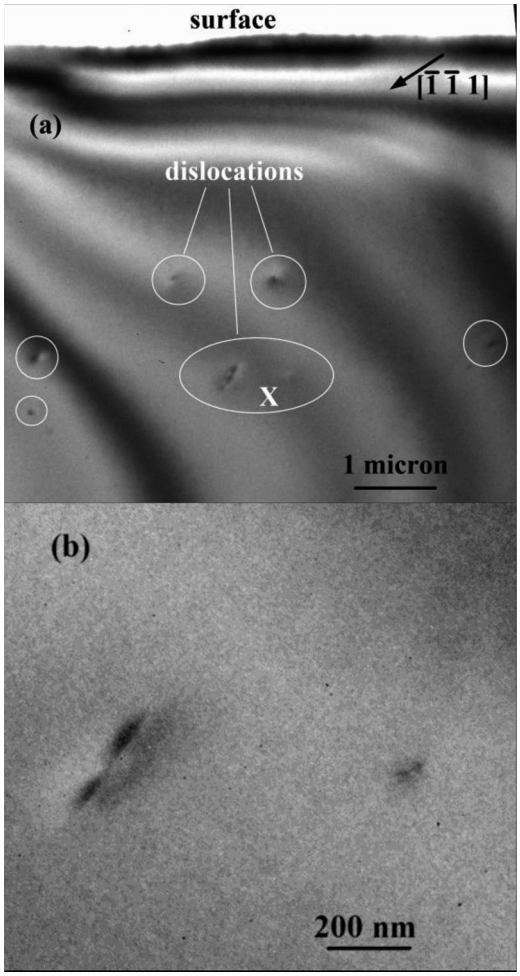

Fig. 7. (a) TEM two-beam [–1 –1 1] bright-field image of the (0 1 1) cross section of the (1 0 0) boron-diffused silicon wafer N3. The [0 1 1] zone-axis is along the beam direction. The dislocations are marked with the white circles, and they form a band parallel to the wafer surface. The broad wavy features are thickness fringes due to the nonuniformity of the thickness of the TEM specimen. (b) Image with higher magnification of the area marked with "X" in (a).

the luminescence from oxygen precipitates, reported by Tajima *et al.* [18] and Bothe *et al.* [42]. However, oxygen precipitates and dislocations often appear together [43] due to the local stress and strain around the precipitates. In addition, Tajima *et al.* [18] reported that oxygen precipitate luminescence was confined around small-angle grain boundaries, which were known to have high dislocation densities, and the luminescence only appeared at 100 K or above. Meanwhile, our defect peak 2 can be observed at 79 K and extends well below the wafer surface compared with the dislocation band. Therefore, the observed luminescence peak is unlikely due to oxygen precipitates, although oxygen precipitates could possibly decorate around the dislocations near the surface.

In fact, defect peak 2 can be compared with the results reported by Charnvanichborikarn *et al.* [44], [45]. These authors found a broad PL band beyond 1400 nm from irradiated c-Si wafers annealed at high temperatures and proposed that this PL band arose from the localized strain in the early stages of extended defect formation or interstitial clusters. In addition, in Fig. 6(a), there is a shifting toward longer wavelengths of defect peak 1 with increasing distances from the edge, which is similar to that of D3 when moving away from the subgrain boundaries in mc-Si [31]. We note that, although the spectrally resolved PLE technique was demonstrated here on boron-diffused layers and dislocations in c-Si wafers, it could, in principle, be applied for others structures and defects separated at different depths within a wafer.

VI. Conclusion

Combining spectrally resolved PL and PLE spectroscopy techniques, we have captured full luminescence spectra with varying excitation wavelengths, allowing us to examine the properties of different layers and defect types at various depths inside boron-diffused silicon wafers. We have demonstrated that this method can be used to qualitatively assess doping concentrations and junction depths. In addition, we have applied this method to detect dislocations induced by the post-diffusion thermal treatment process, giving insightful information about the spatial distribution of both dislocations and secondary defects located below the wafer surfaces.

Acknowledgment

The authors would like to thank Prof. H. Tan for providing access to the spectroscopic equipment; Prof. B. Luther-Davies, Dr. S. Mokkapati, and D. Llewellyn for assisting with the hardware setup; and D. Yan for providing the boron-diffused n-type silicon wafers. The Australian National Fabrication Facility, the Center for Advanced Microscopy, and the Australian Microscopy and Microanalysis Research Facility ACT node are greatly acknowledged for providing access to some of the facilities used in this work.

References

[1] W. Bludau, A. Onton, and W. Heinke, "Temperature dependence of the band gap of silicon," *J. Appl. Phys.*, vol. 45, pp. 1846–1848, 1974.
[2] J. Wagner, "Photoluminescence and excitation spectroscopy in heavily doped n- and p-type silicon," *Phys. Rev. B*, vol. 29, pp. 2002–2009, 1984.
[3] J. Wagner, "Band-gap narrowing in heavily doped silicon at 20 and 300 K studied by photoluminescence," *Phys. Rev. B*, vol. 32, pp. 1323–1325, 1985.
[4] E. Daub and P. Würfel, "Ultralow values of the absorption coefficient of Si obtained from luminescence," *Phys. Rev. Lett.*, vol. 74, pp. 1020–1023, 1995.
[5] T. Trupke *et al.*, "Temperature dependence of the radiative recombination coefficient of intrinsic crystalline silicon," *J. Appl. Phys.*, vol. 94, pp. 4930–4937, 2003.
[6] H. T. Nguyen, F. E. Rougieux, B. Mitchell, and D. Macdonald, "Temperature dependence of the band-band absorption coefficient in crystalline silicon from photoluminescence," *J. Appl. Phys.*, vol. 115, pp. 043710-1–043710-8, 2014.
[7] P. P. Altermatt *et al.*, "Injection dependence of spontaneous radiative recombination in crystalline silicon: Experimental verification and theoretical analysis," *Appl. Phys. Lett.*, vol. 88, pp. 261901-1–261901-3, 2006.
[8] H. T. Nguyen, S. C. Baker-Finch, and D. Macdonald, "Temperature dependence of the radiative recombination coefficient in crystalline silicon from spectral photoluminescence," *Appl. Phys. Lett.*, vol. 104, pp. 112105-1–112105-3, 2014.
[9] M. Tajima, T. Iwai, H. Toyota, S. Binetti, and D. Macdonald, "Donor-acceptor pair luminescence in compensated Si for solar cells," *J. Appl. Phys.,* vol. 110, pp. 043506-1–043506-5, 2011.

[10] B. D. Rezgui, J. Veirman, S. Dubois, and O. Palais, "Study of donor–acceptor pair luminescence in highly doped and compensated Cz silicon," *Phys. Status Solidi A*, vol. 209, pp. 1917–1920, 2012.
[11] P. Würfel *et al.*, "Diffusion lengths of silicon solar cells from luminescence images," *J. Appl. Phys.*, vol. 101, pp. 123110-1–123110-10, 2007.
[12] J. A. Giesecke, M. Kasemann, M. C. Schubert, P. Würfel, and W. Warta, "Separation of local bulk and surface recombination in crystalline silicon from luminescence reabsorption," *Prog. Photovoltaics, Res. Appl.*, vol. 18, pp. 10–19, 2011.
[13] B. Mitchell, M. K. Juhl, M. A. Green, and T. Trupke, "Full spectrum photoluminescence lifetime analyses on silicon bricks," *IEEE J. Photovoltaics*, vol. 3, no. 3, pp. 962–969, Jul. 2013.
[14] C. Barugkin, Y. Wan, D. Macdonald, and K. R. Catchpole, "Evaluating plasmonic light trapping with photoluminescence," *IEEE J. Photovoltaics*, vol. 3, no. 4, pp. 1292–1297, Oct. 2013.
[15] C. Schinke, D. Hinken, J. Schmidt, K. Bothe, and R. Brendel, "Modeling the spectral luminescence emission of silicon solar cells and wafers," *IEEE J. Photovoltaics*, vol. 3, no. 3, pp. 1038–1052, Jul. 2013.
[16] H. T. Nguyen, F. E. Rougieux, S. C. Baker-Finch, and D. Macdonald, "Impact of carrier profile and rear-side reflection on photoluminescence spectra in planar crystalline silicon wafers at different temperatures," *IEEE J. Photovoltaics*, vol. 5, no. 1, pp. 77–81, Jan. 2015.
[17] W. Lee, J. Chen, B. Chen, J. Chang, and T. Sekiguchi, "Cathodoluminescence study of dislocation-related luminescence from small-angle grain boundaries in multicrystalline silicon," *Appl. Phys. Lett.*, vol. 94, pp. 112103-1–112103-1, 2009.
[18] M. Tajima *et al.*, "Deep-level photoluminescence due to dislocations and oxygen precipitates in multicrystalline Si," *J. Appl. Phys.*, vol. 111, pp. 113523-1–113523-6, 2012.
[19] M. Tajima, "Spectroscopy and topography of deep-level luminescence in photovoltaic silicon," *IEEE J. Photovoltatics*, vol. 4, no. 6, pp. 1452–1458, Nov. 2014.
[20] P. Gundel *et al.*, "Micro-photoluminescence spectroscopy on metal precipitates in silicon," *Phys. Status Solidi RRL*, vol. 3, pp. 230–232, 2009.
[21] R. Woehl *et al.*, "Evaluating the aluminum-alloyed p+-layer of silicon solar cells by emitter saturation current density and optical microspectroscopy measurements," *IEEE Trans. Electron Devices*, vol. 58, no. 2, pp. 441–447, Feb. 2011.
[22] P. Gundel *et al.*, "Comprehensive microscopic analysis of laser-induced high doping regions in silicon," *IEEE Trans. Electron Devices*, vol. 58, no. 9, pp. 2874–2877, Sep. 2011.
[23] A. Roigé *et al.*, "Microscale spatially resolved characterization of highly doped regions in laser-fired contacts for high-efficiency crystalline Si solar cells," *IEEE J. Photovoltatics*, vol. 5, no. 2, pp. 545–551, Mar. 2015.
[24] H. T. Nguyen *et al.*, "Dislocations in laser-doped silicon detected by micro-photoluminescence spectroscopy," *Appl. Phys. Lett.*, vol. 107, pp. 022101-1–022101-5, 2015.
[25] H. T. Nguyen *et al.*, "Micro-photoluminescence spectroscopy on heavily-doped layers of silicon solar cells," *Phys. Status Solidi RRL*, vol. 9, pp. 230–235, 2015.
[26] J. Wagner, "Heavily doped silicon studied by luminescence and selective absorption," *Solid-State Electron.*, vol. 28, pp. 25–30, 1985.
[27] J. Wagner, K. Thonke, and R. Sauer, "Excitation spectroscopy on the 0.79-eV (C) line defect in irradiated silicon," *Phys. Rev. B*, vol. 29, pp. 7051–7053, 1984.
[28] M. L. W. Thewalt, S. P. Watkins, U. O. Zlemelis, E. C. Lightowlers, and M. O. Henry, "Photoluminescence lifetime, absorption and excitation spectroscopy measurements on isoelectronic bound excitons in beryllium-doped silicon," *Solid State Commun.*, vol. 44, pp. 573–577, 1982.
[29] M. K. Juhl, T. Trupke, M. Abbott, and B. Mitchell, "Spatially resolved absorptance of silicon wafers from photoluminescence imaging," *IEEE J. Photovoltaics*, vol. 5, no. 6, pp. 1840–1843, Nov. 2015.
[30] D. Yan and A. Cuevas, "Empirical determination of the energy band gap narrowing in p+ silicon heavily doped with boron," *J. Appl. Phys.*, vol. 116, pp. 194505-1–194505-7, 2014.
[31] H. T. Nguyen, F. E. Rougieux, F. Wang, H. Tan, and D. Macdonald, "Micrometer-scale deep-level spectral photoluminescence from dislocations in multicrystalline silicon," *IEEE J. Photovoltaics*, vol. 5, no. 3, pp. 799–804, May 2015.
[32] C. Schinke *et al.*, "Uncertainty analysis for the coefficient of band-to-band absorption of crystalline silicon," *AIP Advances*, vol. 5, pp. 067168-1–067168-22, 2015.
[33] W. P. Dumke, "Comparison of band-gap shrinkage observed in luminescence from n+-Si with that from transport and optical absorption measurements," *Appl. Phys. Lett.*, vol. 42, pp. 196–198, 1983.
[34] P. E. Schmid, M. L. W. Thewalt, and W. P. Dumke, "Photoluminescence in heavily doped Si:B and Si:As," *Solid State Commun.*, vol. 38, pp. 1091–1093, 1981.
[35] E. Arai, H. Nakamura, and Y. Terunuma, "Interface reactions of B2O3-Si system and boron diffusion into silicon," *J. Electrochem. Soc. Solid State Sci. Technol.*, vol. 120, pp. 980–987, 1973.
[36] N. E. Grant and K. R. McIntosh, "Passivation of a (100) silicon surface by silicon dioxide grown in nitric acid," *IEEE Electron Device Lett.*, vol. 30, no. 9, pp. 922–924, Sep. 2009.
[37] P. J. Cousins and J. E. Cotter, "The influence of diffusion-induced dislocations on high efficiency silicon solar cells," *IEEE Trans. Electron Devices*, vol. 53, no. 3, pp. 457–464, Mar. 2006.
[38] M. A. Kessler, T. Ohrdes, B. Wolpensinger, and N.-P. Harder, "Charge carrier lifetime degradation in Cz silicon through the formation of a boron-rich layer during BBr3 diffusion processes," *Semicond. Sci. Technol.*, vol. 25, pp. 055001-1–055001-9, 2010.
[39] H. T. Nguyen, F. E. Rougieux, F. Wang, and D. Macdonald, "Effects of solar cell processing steps on dislocation luminescence in multicrystalline silicon," *Energy Procedia*, vol. 77, pp. 619–625, 2015.
[40] X. J. Ning, "Dislocations induced by boron diffusion in silicon: A transmission electron microscopy study," *Philosoph. Mag. A*, vol. 75, pp. 115–135, 1997.
[41] A. Hara, T. Fukuda, T. Miyabo, and I. Hirai, "Oxygen-nitrogen complexes in silicon formed by annealing in nitrogen," *Appl. Phys. Lett.*, vol. 54, pp. 626–628, 1989.
[42] K. Bothe, R. J. Falster, and J. D. Murphy, "Room temperature sub-bandgap photoluminescence from silicon containing oxide precipitates," *Appl. Phys. Lett.*, vol. 101, pp. 032107-1–032107-4, 2012.
[43] S. Binetti *et al.*, "Optical properties of oxygen precipitates and dislocations in silicon," *J. Appl. Phys.*, vol. 92, pp. 2437–2445, 2002.
[44] S. Charnvanichborikarn *et al.*, "Effect of boron on interstitial-related luminescence centers in silicon," *Appl. Phys. Lett.*, vol. 96, pp. 051906-1–051906-3, 2010.
[45] S. Charnvanichborikarn, J. Wong-Leung, C. Jagadish, and J. S. Williams, "Direct correlation of R-line luminescence with rod-like defect evolution in ion-implanted and annealed silicon," *MRS Commun.*, vol. 2, pp. 101–105, 2012.

Authors' photographs and biographies not available at the time of publication.